Transactions of the Korean Nuclear Society Autumn Meeting
Gyeongju, Korea, October 27-28, 2016

Experimental Study on Boiling Crisis in Pool Boiling

Satbyoul Jung [a] and Hyungdae Kim [a*]
[a]*Nuclear Engineering, Kyung Hee University, Republic of Korea*
[*]*Corresponding author: hdkims@khu.ac.kr*

1. Introduction

Numerous theoretical models to explain the triggering mechanism of critical heat flux (CHF) have been proposed. The hydrodynamic instability model was firstly suggested by Kutateladze [1] and Zuber [2]. They hypothesized that CHF is triggered when velocity difference of vapor and liquid phases at interface is large enough over the critical value to disrupt vapor flow from the heater surface. Meanwhile, Haramura and Katto [3] proposed the macrolayer model based on the observation of thin liquid layer trapped by several vapor stems under a mushroom bubble. In the model, CHF was assumed to occur when the evaporation rate of macrolayer exceeds that the hovering time of mushroom bubble. Based on the macrolayer model, several studies to directly observe the macrolayer and modify the original model proposed by Haramura and Katto [4-5] have been performed. Although these prediction models based on hydrodynamic stability showed reasonable agreements with several experimental data, they could not explain effects of surface wetting on CHF. In this regard, recent studies have focused on observing the wetting behavior near the contact line, resulting in observation in micron-scale near a wall. Theofanous *et al*. [6] observed growth of a hot patch, leading to burn out, by measuring the local wall temperature distribution using the infrared (IR) thermometry technique. They postulated that failure in re-wetting of a dry patch by a cooling liquid is governed by micro-hydrodynamics near the wall. On the other hand, Chu *et al.* [7] suggested the CHF triggering mechanism based on their observations about the formation of a residual dry patch using the total reflection (TR) technique. Chu *et al.* [7] commonly observed that active coalescence of newly generated bubbles with preexisting bubbles results in a residual dry patch and prevents the complete rewetting of the dry patch, leading to CHF. Although each observation provides some insights about CHF triggering mechanisms, there is still a deficiency in developing the mechanistic prediction model of CHF without consideration about the coupled effects of hydrodynamics and thermal behavior in relation with rewetting of dry patches.

In this work, to reveal the key physical mechanism of CHF during the rewetting process of a dry patch, dynamics of dry patches and thermal pattern of a boiling surface are simultaneously observed using TR and IR thermometry techniques.

2. Experimental Method

In this section, an integrated visible and infrared-based experimental method is introduced to simultaneously measure temperature and phase distributions on a heated wall [8].

2.1 Test sample

In order to ensure the optical techniques, we consider a thin film electric heater on a base plate as the test sample. For visible light, both the film heater and the base plate are transparent to implement TR technique. For infrared light, the base plate is transparent whereas the film heater is non-transparent, so that the thermal image of the heater surface can be captured from below the base plate. A good example is the combination of an Indium-Tin-Oxide (ITO) thin film heater (transparent to visible and opaque to infrared lights) and a sapphire plate (transparent to both visible and infrared lights), which is used for this study.

2.2 Experimental setup

Figure 1 shows the schematic of the optical setup. The temperature distribution of the boiling surface is measured using an IR camera placed below the base plate. Simultaneously the phase distribution on the boiling surface is detected using the TR technique with a high speed video (HSV) camera. The image obtained by the TR technique appears dark for liquid phase and bright for vapor phase. The IR and HSV cameras were temporally synchronized using a function generator. The obtained each images could be spatially mapped by capturing a reference dots on test sample. In addition, another HSV camera and high flux LED were installed to visualize the bubble dynamics from side. The frame rates of IR and HSV cameras were at 500 Hz and 5 kHz, respectively.

2.3 Numerical processing for heat flux

Transient heat conduction equation for the heater plate was numerically solved by using the measured time-varying temperature distribution data of the boiling surface as boundary conditions using a commercial CFD program (ANSYS-CFX) and a user defined code which was added to update the temperature boundary condition on the boiling surface for each time step.

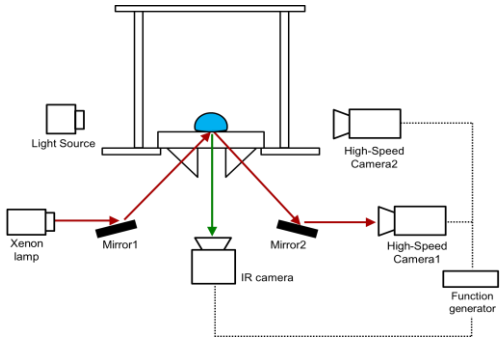

Fig. 1. Schematic of the optical system

3. Results and Discussions

3.1 Boling curve

All the data presented in this paper were obtained for nucleate boiling of saturated water under atmospheric pressure. Figure 2(a) shows the boiling curve of the time and area averaged heat flux and temperature, which is obtained by controlling the power to ITO heater. It shows the general behavior on nucleate boiling regime. Once over the CHF, the local temperature extremely rises up over 1000°C within few seconds, as seen in Fig. 2(b). In order to investigate the triggering mechanism of CHF leading to burnout, the local measurement of dynamics of dry spot and corresponding thermal characteristics at each heat flux was performed using the integrated method of TR and IR thermometry techniques.

3.2 Transient area fraction and local wall temperature

Figure 3 shows the transient dry area fraction and maximum temperature at each heat flux, respectively. As expected, the dry area fraction and maximum temperature increase with the applied heat flux because the coalescence of dry patch become more active as increasing the heat flux. However, the wide fluctuation is observed at high heat fluxes. At the CHF, the abnormal increase of both temperature and area fraction sometimes occurs and eventually it goes through the irreversible increase. Therefore, we focus on the initiation of abnormal increase of temperature and dry fraction, triggering the irreversible dry patch (0.5-1.0s).

3.3 Observation of rewetting failure phenomenon

Figure 4 shows transient maximum temperature and dry area fraction with focus on initiation of the irreversible dry patch. Figure 5 shows the sequential visualization images corresponding to the bubble dynamics from side, liquid-vapor phase distribution, and temperature distribution. In liquid-vapor phase distribution, the bright area corresponds to the vapor phase and the dark area indicates liquid phase.

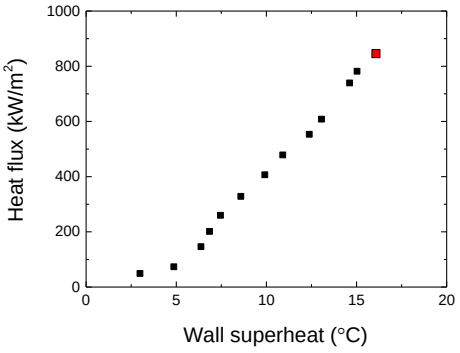

(a)

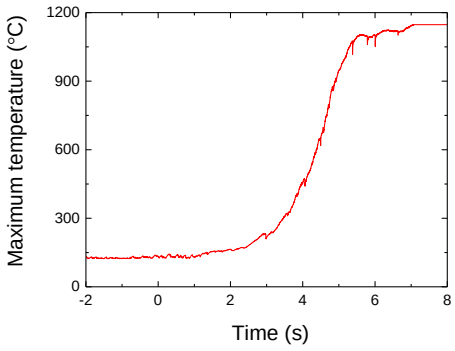

(b)

Fig. 2. (a) Boiling curve; (b) transient maximum temperature at the CHF

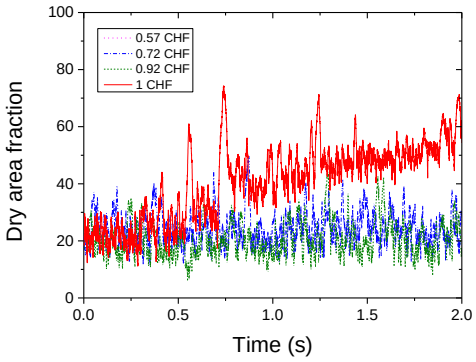

(a)

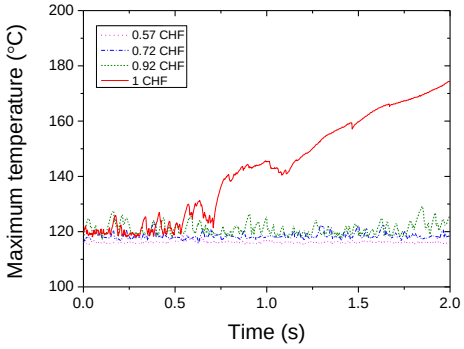

(b)

Fig. 3. (a) Dry area fraction history (frame rate = 5 kHz); (b) maximum wall temperature history (frame rate = 500 Hz)

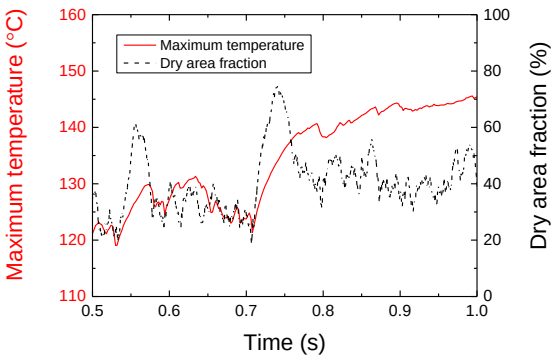

Fig. 4. Transient temperature and dry area fraction focused on initiation of the irreversible hot patch

The triple contact line (TCL) could be extracted from the phase distribution data and the obtained TCL data was superimposed on the local wall temperature distribution.

At 0.69s, several dry patches are formed, they grow larger. And then they make a large dry patch at 0.73s. The dry area fraction is about 75% and the surface locally dried out over 130°C, although the time- and area- averaged temperature is ~117°C. Then, it is rewetted by liquid (0.75-0.79s). However, it is observed that the dry patch is not completely rewetted due to the failure of liquid rewetting, even though the mushroom bubble departs from the wall at 0.79s. The thermal energy is accumulated to remaining dry patch, resulting in the local dry out at the center of one (>140°C). The next rewetting again fails to completely extinguish the hot patch, repeating to expand and contract, as seen in Fig. 4. Finally, the patch irreversibly grows and leads to transition to film boiling.

3.4 Cause of rewetting failure

Using the local heat flux distribution, the bubble nucleation could be clearly observed. In the local heat flux images (Fig. 6), the area shows very high heat flux over 1.5 MW/m^2, obviously due to bubble nucleation and evaporation of microlayer. In contrast, very low heat fluxes close to zero correspond to the dried area. The sequence images for local heat flux shows details at which the dry patch fails to be rewetted.

The liquid front advances and dry patch contracts (0.788-0.794s). At 0.796s, it is observed that the bubbles actively are nucleated near the advancing TCL, while the nucleation at bulk liquid is relatively small. After that event, the dry patch expands due to the coalescence of newly generated dry spots near the TCL. When the temperature of a dry patch under a growing massive bubble rises beyond the instantaneous nucleation temperature, the bubbles instantaneously nucleate at the head of the advancing liquid meniscus and prevents the liquid front advancing under the departing massive bubble, and consequently the overheated dry patch is not extinguished after the departure of the massive bubble.

Based on the aforementioned observations, it is hypothesized that the nucleation characteristics at the TCL plays a key role in the rewetting process of dry patches. In order to analyze the relation between the number of nucleation site near the TCL and rewetting behavior, line nucleation site density (LNSD) around a dry patch is newly introduced. As seen in Fig. 7 (a), the LNSD is maximum at 0.796 s at which the liquid front advancing is prevented (Fig. 6). The maximum LNSD increases as the applied heat flux increases, as seen in Fig. 7 (b). The values are reasonable in order of magnitude, compared to Paul and Abdel-Khailk's empirical correlations [9] for LNSD. And interestingly,

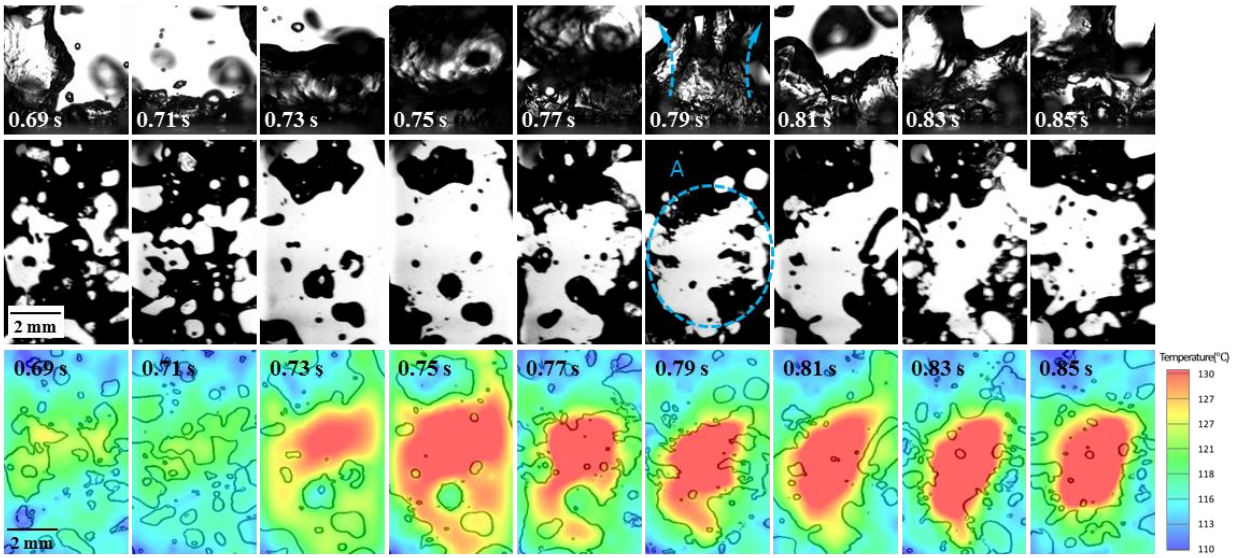

Fig. 5 Boiling behaviors at the boiling crisis; bubble dynamics from side, liquid-vapor phases distribution on the wall and local wall temperature distribution

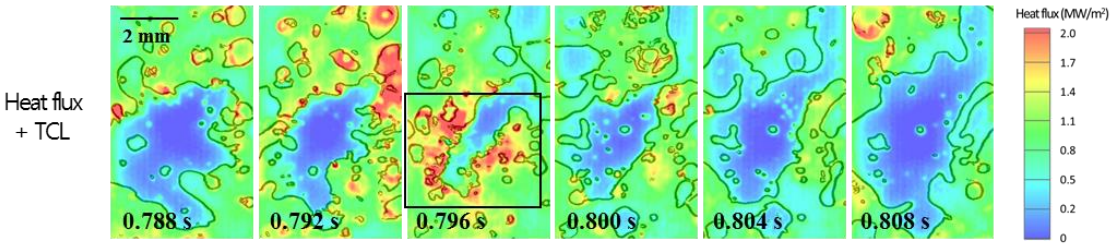

Fig. 6 Local heat flux distribution on boiling surface at boiling crisis, showing the instantaneous bubble nucleation near TCL

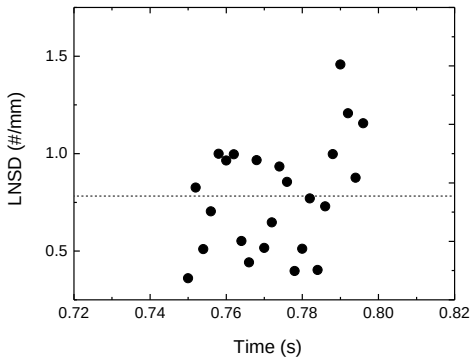

(a)

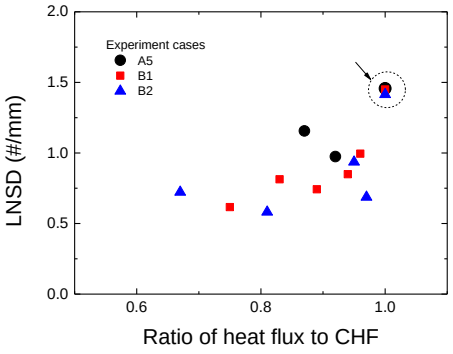

(b)

Fig. 7. (a) instantaneous LSND with time; (b) maximum LSND with applied heat flux for three experiment cases

the maximum LNSD values in three experiment cases are almost same as ~1.5 #/mm. In order to understand exact triggering mechanism of CHF, a detailed analysis of LNSD is necessary.

3. Conclusions

Local dynamics of dry patch and thermal pattern on a boiling surface in synchronized manner for both space and time using TR and IR thermometry were measured during pool boiling of water. Observation and quantitative examination of CHF was performed. The main contributions of this work are summarized below.

- The hydrodynamic and thermal behaviors of irreversible dry patch were observed. The dry patches coalesce into a large dry patch and it locally dried out. Due to the failure of liquid rewetting, the dry patch is not completely rewetted, resulting in the burn out at which temperature is ~140°C.
- When temperature of a dry patch rises beyond the instantaneous nucleation temperature, several bubbles nucleate at the head of the advancing liquid meniscus and prevents the liquid front, and eventually the overheated dry patch remains alive after the departure of the massive bubble.
- LNSD plays a key role in the rewetting capability. In our experimental cases, the maximum LNSD values at CHF are almost same as ~1.5 #/mm.

REFERENCES

[1] S. S. Kutateladze, On the Transition to Film Boiling Under Natural Convection, Kotloturbostroenie, Vol. pp. 152-180, 1948.
[2] N. Zuber, Hydrodynamic Aspects of Boiling Heat Transfer, Ph.D. thesis, UCLA, USA, 1959.
[3] Y. Haramura and Y. Katto, A new hydrodynamic model of critical heat flux, applicable widely to both pool and forced convection boiling on submerged bodies in saturated liquids, Int. J. Heat Mass Transfer, Vol. 26, No. 3, pp. 389–399, 1983.
[4] I. C. Bang, S. H. Chang and W. Baek, Visualization of a Principle Mechanism of Critical Heat Flux in Pool Boiling, Int. J. Heat Mass Transfer, Vol. 706, No. 48, pp. 5371–5385, 2005.
[5] H. S. Ahn and M. H. Kim, Visualization Study of Critical Heat Flux Mechanism on a Small and Horizontal Copper Heater, Int. J. Multiphase Flow, Vol. 710, No. 41, pp. 1–12, 2012.
[6] T. G. Theofanous, T. N. Dinh, J. P. Tu, and A. T. Dinh, The Boiling Crisis Phenomenon Part I: Nucleation and Nucleate Boiling Heat Transfer, Exp. Therm. Fluid Sci., Vol. 26, pp. 775–792, 2002.
[7] I. Chu, H. C. No, C. Song, Visualization of Boiling Structure and Critical Heat Flux Phenomenon for a Narrow Heating Surface in a Horizontal Pool of Saturated Water, Int. J. Heat and Mass Transfer, Vol. 62, pp. 142–152, 2013.
[8] S. Jung, H. Kim, An Experimental Method to Simultaneously Measure the Dynamics and Heat Transfer associated with a Single Bubble during Nucleate Boiling on a Horizontal Surface, Int. J. Heat and Mass Transfer, Vo. 73, pp. 365-375, 2014.
[9] D. D. Pual and S. I. Abdel-Khalik, A Statistical Analysis of Saturated Nucleate Boiling along a Heated Wire, Int. J. Heat Mass Transfer, Vol. 26, No. 4, pp. 509-519, 1983.